Atmospheric Speciated Mercury Concentrations on an Island between China and Korea: Sources and Transport Pathways

Gang-San Lee[1], Pyung-Rae Kim[1], Young-Ji Han[11], Thomas M. Holsen[2], Yong-Seok Seo[3,4], Seung-Muk Yi[3]

[1]Department of Environmental Science, College of Natural Science, Kangwon National University, 1 Kangwondaehak-gil, Chuncheon, Kangwon-do, 200-701, Republic of Korea

[2]Department of Civil and Environmental Engineering, Clarkson University, 8 Clarkson Ave., Potsdam, NY 13699-5710, USA

[3]Department of Environmental Health, Graduate School of Public Health, Seoul National University, Gwanak-ro, Gwanak-gu, Seoul 151-742, Republic of Korea

[4]Institute of Health and Environment, Seoul National University, 1 Gwanak-ro, Gwanak-gu, Seoul 151-742, Republic of Korea

[1] Correspondence to: Y.J. Han (youngji@kangwon.ac.kr)

Abstract

As a global pollutant, mercury (Hg) is of particular concern in East Asia where anthropogenic emissions are the largest. In this study, speciated Hg concentrations were measured on Yongheung Island, the western most island in Korea, located between China and the Korean mainland to identify the importance of local and regional Hg sources. Various tools including correlations with other pollutants, conditional probability function, and back-trajectory based analysis consistently indicated that Korean sources were important for gaseous oxidized mercury (GOM) whereas, for total gaseous mercury (TGM) and particulate bound mercury (PBM), regional transport were also important. A trajectory cluster based approach considering both Hg concentration and the fraction of time each cluster was impacting the site was developed to quantify the effect of Korean sources and out-of-Korean source. This analysis suggests that contributions from out-of-Korean sources were similar to Korean sources for TGM whereas Korean sources contributed slightly more to the concentration variations of GOM and PBM compared to out-of-Korean sources. The ratio of GOM/PBM decreased when the site was impacted by regional transport, suggesting that this ratio may be a useful tool for identifying the relative significance of local sources vs. regional transport. The secondary formation of PBM through gas-particle partitioning with GOM was found to be important at low temperatures and high relative humidity.

***Keywords** : TGM, GOM, PBM, regional transport, gas-particle partitioning, cluster analysis*

1. Introduction

Mercury (Hg) is the only metal that exists as a liquid at standard conditions (US EPA, 1997) which results in it having a significant vapor pressure and presence in the atmosphere. In the atmosphere, Hg generally does not constitute a direct public health risk at the level of exposure usually found (Driscoll et al, 2007). However, once Hg is deposited into aquatic systems, it can be transformed into methyl-mercury (MeHg) which is very toxic and readily bioaccumulates through the food web (Mason et al.,

1995). Many studies show that one of the major sources of MeHg in aquatic and terrestrial system is atmospheric deposition of inorganic Hg (Landis and Keeler, 2002, Mason et al., 1997). Fish consumption has been considered to be the major exposure pathway of Hg for humans (Mergler et al., 2007; UNEP, 2013). In Korea, You et al. (2012) showed that MeHg concentrations in blood were affected by fish consumption as well as by gender difference. However, rice consumption was also found to be the predominant pathway of MeHg exposure for the inhabitants residing in a highly contaminated area of China (Zhang et al., 2010).

Atmospheric mercury exists in three major inorganic forms, including gaseous elemental mercury (GEM, Hg^0), gaseous oxidized mercury (GOM, Hg^{2+}) and particulate bound mercury (PBM, Hg(p)). The sum of the GEM and GOM is often called as total gaseous mercury (TGM). Due to its high water solubility and deposition velocity, GOM has short atmospheric residence times (~day) and, consequently, its ambient concentration is mainly affected by local sources. Besides the anthropogenic sources, the free troposphere has been identified as an important GOM source (Huang and Gustin, 2012; Weiss-Penzias et al., 2009; Timonen et al., 2013). In contrast, GEM, which comprises more than 95 percent of the total Hg in ambient air, can be transported long distances because it is relatively inert and has low water solubility and deposition velocity (Lin and Pehkonen, 1999). The residence time of PBM is dependent on the size of associated particles, but generally, it has been assumed to be a few days (Fang et al., 2012, Zhang et al., 2001). Measurements of GOM and PBM are challenging and uncertain due to their extremely low concentrations and complex chemical reactivity, and because their chemical forms are not actually known (Pirrone et al., 2013). In most studies, GOM and PBM have operational definitions for the mercury species collected by a KCl coated denuder and by a quartz filter downstream of a KCl denuder, respectively. It is typically assumed that GOM comprises $HgCl_2$, $HgBr_2$, HgO, $Hg(NO_3)_2$, and $HgSO_4$. However, the sampling method including the use of a KCl denuder has been shown to be subject to interferences from ozone, water vapor and possibly other compounds (Lyman et al. 2010; Talbot et al., 2011; Jaffe et al., 2014; Finley et al., 2013; Gustin et al., 2013; Huang et al., 2013; McClure et al., 2014), and it also should be noted that the different Hg(II) compounds have different collection efficiencies by the KCl coated denuder (Gustin et al.,

2015).

In the atmosphere, Hg species can be interconverted through various redox reactions. It is known that GOM can be produced by homogeneous and heterogeneous reactions of GEM with O_3, OH, and Br/BrO (Hedgecock and Pirrone, 2004; Obrist et al., 2011; Subir et al., 2011), but there is no consensus on which oxidants are most important under which environmental conditions. GEM can also be formed through reduction of GOM predominantly in cloud water (Subir et al. 2011, 2012). GOM can also be converted to PBM through gas-particle partitioning, with the partition coefficient, K_p, inversely correlated with temperature and positively correlated with particle surface area (Lyman and Keeler, 2005, Rutter and Schauer, 2007a,b; Liu et al., 2010). Since GEM makes up the bulk of the total Hg in ambient air its formation through reduction processes of divalent Hg may not be important. However, the secondary formations of GOM through the oxidation of Hg^0 followed by gas-particle partitioning formation of PBM can contribute significantly to their ambient concentrations.

The region of largest anthropogenic Hg emissions is East and Southeast Asia, contributing 39.7% of the total global anthropogenic emissions (UNEP, 2013). In Korea, atmospheric Hg emissions have generally decreased since 1990 (Kim et al., 2010). However, Hg levels in Korea are likely to be highly susceptible to Chinese emissions because China alone accounts for about one third of the global total (UNEP, 2013) and Korea is situated just east (and generally downwind) of China. According to the recent studies, Hg concentrations in blood of Koreans are more than 4~8 times higher than those found in US and Germany, and approximately 26% of Koreans have higher blood mercury concentrations than a USA guideline level (http://envhealth.nier.go.kr), indicating that there is an urgent need to identify the Hg sources and pathways controlling Hg concentrations in Korea.

This study was designed to identify the contribution of various Hg sources including direct emissions from anthropogenic and natural sources and indirect secondary formation processes to atmospheric Hg concentrations in Korea. In order to achieve these objectives, Hg concentrations were measured in the western most island in Korea, located in between eastern China and the Korean mainland, so that, depending on wind patterns, the effects of Chinese and Korean Hg emissions could be evaluated. Previously, our group qualitatively evaluated the impact of local Korean sources and

regional Chinese sources on TGM concentrations at the same sampling site (Lee et al. 2014). However, that work was unable to identify the effect of sources on Hg levels in Korea because only TGM was measured whereas all three Hg species are needed since they have very different physical and chemical properties. In this study, the importance of sources and pathways were both qualitatively and quantitatively evaluated using all three Hg species' concentrations measured throughout the extended sampling period.

2. Materials and methods

2.1 Site description

TGM, GOM and PBM were measured on the roof of a three-story building on Yongheung Island (YI), the westernmost island in Korea (Fig. 1). YI is a small island located about 15~20 km west from mainland Korea with a population of 5,815. The Yongheung Coal-fired Power Plant (YCPP), located approximately 4.5 km southwest of the sampling site (Fig 1c), emits about 0.11 ton yr^{-1} of Hg. To the east of the sampling site, industrial (the Incheon industrial complex shown as light violet color in Fig 1b and Fig 1c) and metropolitan (Seoul shown as a pink color in Fig 1b and Fig 1c) areas are located in mainland Korea, and, in the southern direction, there are three large coal fired power plants (Fig 1b). The Hg emission rate of anthropogenic sources in Korea was estimated to be 8.04 ton yr^{-1} in 2010, with cement production being the largest source type (AMAP/UNEP, 2013).

2.2 Sampling and analysis

From January 2013 to August 2014, three atmospheric mercury species: TGM (GEM+GOM), GOM, and PBM (≤2.5 μm) were measured during eight intensive sampling periods (Table 1). TGM concentrations were measured every 5 min using a mercury vapor analyzer (Tekran 2537B). This instrument contains two gold cartridges which collect and thermally desorb Hg alternately. Desorbed Hg is quantifed using cold vapor atomic fluorescence spectrometry (CVAFS). Outdoor air at a flow rate of 1.0 L min^{-1} was transported through a 3-m-long heated sampling line (1/4" OD Teflon) into the analyzer. There is a possibility that some of GOM may be sorbed in the line upstream of the gold traps

although the sampling line and inlet were maintained at 50^{o}C to prevent the GOM sorption. However, it is typically assumed that Tekran 2537 can collect and analyze TGM in most of studies (Temme et al., 2002; Gustin et al., 2013; Han et al., 2014; Zhang et al., 2015). The Tekran 2537B was automatically calibrated daily using an internal permeation source. Manual injections were also used to evaluate these automated calibrations before each sampling campaign using a saturated mercury vapor standard. The relative percent difference between manual injection and automated calibration was <2%. Five-point manual calibration was also performed by injecting Hg vapor into the sampling line two times during the study period. The R^2 ranged from 0.9991 to 0.9997 between mass injected and Tekran reported area, and the average relative percent difference between the mass injected and the mass calculated was 5.5%. The method detection limit (0.04 ng m^{-3}) was calculated as three times the standard deviation obtained after injecting 1 pg of the mercury vapor seven times. The recovery rate (96 ± 3%) was obtained by directly injecting Hg vapor into the sampling line between the sample inlet and the Tekran 2537B in a zero-air stream.

GOM and PBM were collected manually using an annular denuder coated with KCl followed by a quartz filter, respectively, at a flow rate of 10 L min^{-1}. To identify any diurnal variations, all samples were separately collected during the daytime (07:00-19:00) and nighttime (19:00-07:00) except during the 7th sampling period when they were measured every 2 hrs. The sampling system including an elutriator, an impactor, a KCl-coated denuder and a filter pack was housed in a custom-made sampling box maintained at 45^{o}C to prevent hydrolysis of KCl. After sampling, the denuder and quartz filter were thermally desorbed using a tube furnace at 525^{o}C and 900^{o}C, respectively, to convert Hg^{2+} to Hg^{0} in a carrier gas of zero air. The heated air was then transported into a Tekran 2537B for quantification. Field blanks for GOM and PBM were collected once for each sampling period, and their average values were 0.23 ± 0.12 pg m^{-3} and 0.25 ± 0.09 pg m^{-3}, respectively.

The sampling methods used in this study are currently the most accepted methods for the measurement of atmospheric GOM and PBM, however there are many studies reporting that these methods are subject to interferences from ozone, water vapor and possibly other compounds (Lyman et al. 2010; Talbot et al., 2011; Jeff et al., 2014; Finley et al., 2013; Gustin et al., 2013; Huang et al.,

2013; McClure et al., 2014) although recent side-by-side measurements with two Tekran systems showed good agreement and no impact from added ozone and increasing relative humidity (Edgerton, personal communication). Also, it should be noted that the concentrations of PBM measured during 12-hrs of sampling time (all sampling periods except in the 7th) may have been biased due to Hg loss from filters over the long sampling period; however for model development any loss of PBM is assumed to be the same for each sampling period. Therefore, it should be noted that the GOM and PBM measurements reported in this study may be somewhat biased even though, at present, it is not possible to quantify the magnitude of these uncertainties.

Meteorological data including temperature, wind speed, wind direction, relative humidity and solar radiation were also measured every 5 min at the sampling site using a meteorological tower (DAVIS Inc weather station, Vintage Pro2^{TM}).

Hourly concentrations of SO_2, NO_2, CO, O_3 and PM_{10} were obtained from the national air quality (NAQ) monitoring station (http://www.airkorea.or.kr/) located approximately 8 km east from the sampling site. These concentrations were compared with those measured at another national air quality monitoring station located approximately 24 km west of the Hg sampling site, and there were no statistical differences between sites (p-value< 0.001), indicating that the spatial distribution of these pollutants was relatively uniform across the area

2.3. Backward trajectory and Cluster analysis

Three-day backward trajectories were calculated using the NOAA HYSPLIT 4.7 with GDAS (Global Data Assimilation System) meteorological data which supplies 3-hour, global 1 degree latitude-longitude datasets of the pressure surface. Hourly 3-day back-trajectories were calculated for each hour of sampling, and the arrival heights of both 200 m and 500 m were used to describe the local and the regional transport meteorological pattern. Since GOM and PBM were measured for 12hr for most time periods, hourly trajectories were matched to the 12hr-averaged GOM and PBM concentration; therefore, in total 12 back-trajectories represented one averaged GOM or PBM concentrations. The different temporal resolution between trajectory and concentration data might

increase the uncertainty of trajectory-based approaches; however, there have been many successful studies using different time scales for measurements of pollutants and for meteorological data (Amato and Hopke, 2012; Galindo et al., 2011; Kim et al., 2007).

The backward trajectories were clustered into groups with similar transport patterns using NOAA HYSPLIT 4.7. This method minimizes the intra-cluster differences among trajectories while maximizing the inter-cluster differences. The clustering of trajectories is based on the total spatial variance (TSV) method. TSV is the sum of all the cluster spatial variances (SPVAR) which is the sum of the squared distances between the endpoints of the cluster's component trajectories and the mean of the trajectories in that cluster. In this study, five clusters were chosen based on a large increase in TSV for larger clusters (Fig. 4S), as described in Draxler et al. (2014) and Kelly et al. (2012). A more detailed description of the clustering process can be obtained in Draxler et al. (2014).

2.5. Conditional Probability Function (CPF)

The conditional probability that a given concentration from given wind direction will exceed a predetermined threshold criterion, was calculated using the following equation.

$$CPF_{\Delta\theta} = \frac{m_{\Delta\theta}}{n_{\Delta\theta}} \quad \text{(Eq.1)}$$

where $m_{\Delta\theta}$ is the number of occurrences from wind sector $\Delta\theta$ where the concentration is higher than a criterion value, and $n_{\Delta\theta}$ is the total number of occurrence from this wind sector. In this study, 16 sectors were used ($\Delta\theta = 22.5^{o}$), and calm winds were excluded from the calculation because of isotropic behavior of the wind vane for such conditions. For TGM, two threshold criteria of the upper 10 and 25 percentile were chosen while only the upper 25 percentile was used for GOM and PBM concentrations due to the smaller number of samples. The 1hr-averaged wind direction (WD) data were used for 12hr-averaged GOM and PBM concentrations for most of periods, so that in total 12 WS and WD were used for one averaged GOM and PBM concentrations to create CPF.

2.6. Potential Source Contribution Function (PSCF)

The PSCF model counts each trajectory segment endpoint that terminates within given grid cell. A

high PSCF value signifies a potential source location. The PSCF value was calculated as:

$$\text{PSCF value} = \frac{P[B_{ij}]}{P[A_{ij}]} = \frac{m_{ij}}{n_{ij}} \quad \text{(Eq.2)}$$

If N is the total number of trajectory segment endpoints over the study period and if n segment trajectory endpoints fall into the ijth cell, the probability of this event ($P[A_{ij}]$) is calculated by n_{ij}/N. If m_{ij} is the number of segment endpoints in the same ijth cell when the concentrations are higher than a criterion value, the probability of this high concentration event, B_{ij}, is given by $P[B_{ij}] = m_{ij}/N$. The criterion value was the top 25% concentration and the cell size of 0.5° by 0.5° was used for tracing sources. To reduce the uncertainty in a grid cell with a small number of endpoints, an arbitrary weight function W_{ij} was applied when the number of the endpoints in a particular cell was less than three times the average number of endpoints (N_{ave}) for all cells (Fu et al., 2011, Han et al., 2007, Polissar et al., 2001a, 2001b).

$$W_{ij} = \begin{pmatrix} 1.0 & N_{ij} > 3N_{ave} \\ 0.70 & 3N_{ave} > N_{ij} > 1.5N_{ave} \\ 0.40 & 1.5N_{ave} > N_{ij} > N_{ave} \\ 0.20 & N_{ave} > N_{ij} \end{pmatrix} \quad \text{(Eq. 3)}$$

In this study, trajectories were hourly calculated

3. Results and discussion

3.1. General trends of three Hg species

To maintain the consistency of the sampling duration, the 12hr-averaged GOM and PBM concentrations were used for the 7th sampling period to identify the general trends of Hg species. The average TGM, GOM, and PBM concentrations were 2.8 ± 1.1 ng m^{-3}, 8.3 ± 9.7 pg m^{-3}, and 10.9 ± 11.2 pg m^{-3}, respectively (Table 1). Since the GOM concentration was much lower than TGM the reported TGM concentration can be considered a good approximation of the GEM concentration. TGM varied from 0.1 to 18.8 ng m^{-3}; the highest concentration was observed around 2 am on March 18, 2014 (Fig. 2). GOM and PBM concentrations peaked at 50.9 pg m^{-3} during the daytime on March 19, 2014 and 43.7 pg m^{-3} during daytime on January 22, 2013, respectively (Fig. 2). The various Hg species did not follow similar concentration patterns although PBM was statistically significantly

241 correlated with TGM (Pearson correlation coefficient, r= 0.235, p-value= 0.03).

242 When the data were grouped into three categories including the first (Apr., 2013, May, 2013, Mar.,
243 2014, May, 2014), the second (Aug, 2013, Aug., 2014.), and the third (Jan., 2013, Feb., 2013) periods,
244 both TGM (ANOVA/Tukey test, p-value<0.001) and PBM (p-value=0.024, Kruska-Wallis test) had
245 the highest concentrations in cold period ((Jan., 2013, Feb., 2013) while there was no statistical
246 difference in GOM concentrations among different categories (p-value= 0.288, Kruskal-Wallis test)
247 (Fig. 3). Observed TGM concentrations were substantially lower than those measured in a suburban
248 and remote site in China and metropolitan areas of Korea (Seoul), but higher than at most North
249 American sites and at a rural site of Korea (Chuncheon) (Table 2). GOM and PBM concentrations
250 were in between those typically found at urban locations and at a rural site in Korea and were much
251 lower than those typically measured in China.

252 The TGM concentration varied diurnally, generally showing morning maximums (07:00-12:00) and
253 minimums during the nighttime. In urban areas, TGM concentrations are typically higher during the
254 nighttime due to a combination of decreased GEM loss by daytime oxidation ,increased use of
255 household heating systems and decreased mixing heights at night (Kim et al., 2012; Han et al., 2014).
256 In contrast daytime peaks have been observed in rural and remote areas, likely due to increased
257 volatilized of Hg^0 from natural sources (Choi et al., 2008; Cheng et al., 2014). Overall these results
258 suggest that TGM concentrations at this site are elevated due to the proximity of regional sources and
259 daily variations are controlled by natural emissions from the ocean and soil surfaces.

260 GOM concentrations were the highest in spring (10.7±10.1 pg m^{-3}) and the lowest in summer

261 (6.2±4.9 pg m^{-3}) with statistically insignificant seasonal variation (Fig. 3). The lack of a GOM
262 seasonal variation for could be an indicator of insignificant secondary formation through
263 photochemical oxidation reactions, but it might be also be due to the small sample numbers and/or
264 relatively long sampling duration (12hr). PBM concentrations did have statistically significant
265 seasonal variations with the highest average concentration in winter (17.8±16.7 pg m^{-3}) and the lowest
266 average concentration in summer (5.8±4.1 pg m^{-3}) (Fig. 3). Higher PBM concentrations in winter
267 were likely caused by increased biomass burning and residential heating, decreased removal from the

atmosphere due to the lower precipitation depth, and/or lower temperatures which favor partitioning to the aerosol phase. Previous studies also often observed the highest PBM concentrations in winter (Mao et al., 2012; Amos et al., 2012; Lan et al., 2012).

In Korea emissions of PBM from anthropogenic sources are much smaller then gaseous emissions (the proportion of GEM, GOM, and PBM released are 64.4%, 28.8%, and 6.8%)(Kim et al., 2010). The fact that PBM concentrations are similar to GOM even though significantly less PBM is released suggests that a significant portion of atmospheric PBM may be due to secondary formation through gas-particle partitioning. This process is characterized by a partition coefficient, $K_{p,}$ which is inversely correlated with temperature (Rutter and Schauer, 2007), possibly causing the distinct seasonal variation in PBM concentrations at the sampling site.

The relationship between K_p, defined as:

$$K_p = \frac{PBM/PM}{Hg_{gas}} \quad \text{(Eq. 4)}$$

where PM represents the particle mass, and Hg_{gas} is the concentration of gaseous Hg and relative humidity (RH) was examined (PM10 concentration was used for PM in Eq. 4 in this study). RH was included since in recent studies K_p was found to increase at high relative humidity in colder seasons (Lyman and Keeler, 2005; Liu et al., 2010). Note that the sampling site was located in a coastal area with generally high RH.

Some previous studies suggested that all gaseous mercury species including Hg^0 may deposit on particles (Xiu et al., 2005; 2009); however, others suggested that the gas-particle partitioning of GOM occurred but assumed that the adsorption of Hg^0 on particles was negligible due to its high vapor pressure (Amos et al., 2012; Rutter and Schauer, 2007). Consistent with this hypothesis, we found a statistically significant multiple linear relationship between K_p with temperature and relative humidity (Fig. 4):

$$\mathrm{Log}(K_p) = -2.518 - 0.036(\mathrm{T}) + 0.017(\mathrm{RH}) \quad \text{(Eq. 5)}$$

where T and RH indicate atmospheric temperature (^{o}C) and relative humidity (%), respectively. The multiple linear equation fit the data well (R^2=0.29, R=0.54, p-value<0.001), and both variables of temperature and relative humidity were statistically significant (p-value<0.001). When each of the

temperature and the RH was used as a single independent variable the log(K_p) regression equation was still significant with a Pearson correlation coefficient of -0.42 (p-value<0.001) and 0.39 (p-value< 0.001), somewhat lower than that from the multiple regression (Fig. 1S). Amos et al. (2012) found an empirical gas-particle partitioning relationship between K_p and T using the Hg data obtained from five monitoring sites in United States and Canada and two laboratory experiments, and average equation is :

$$\mathrm{Log}(K_p) = (10 \pm 1) - (2500 \pm 300)/T \qquad \text{(Eq. 6)}$$

where T is in Kelvin unit. When a partial linear regression was performed with T in this study similar equation was derived: *Log (K_p) = 13.5 – 3362.7/T*. In Amos et al. (2012), the coefficients, ß and y_0, ranged from -1600 to -3300 and 6 to 13, respectively, and R^2 ranged from 0.16 to 0.57 in different monitoring sites, suggesting that the values derived in this study fall into the reasonable range. Somewhat lower R^2 in this study is probably caused by smaller number of samples, different composition of aerosol, different GOM species, and/or longer sampling duration.

Han et al. (2014) also found a significant multiple linear relationship between the ratio of PBM/GOM with temperature and relative humidity at a rural site (R^2= 0.613, ß for T= -0.774, ß for RH= 0.33) but not at an urban site. The lower correlation coefficient and the beta values found in this study compared to those from Han et al. (2014) is probably due to the greater impact of primary anthropogenic sources around the sampling site. A large anthropogenic source near the sampling site is likely to weaken the relative contribution of gas-particle partitioning (secondary formation) to the variations of ambient PBM and GOM concentration because both Hg species can be also strongly affected by the primary source emission. In the study of Amos et al. (2012), the highest R^2 was shown in Experimental Lakes Area of Canada and Reno, NV where no large anthropogenic sources of Hg is located.

In previous researches, GOM concentration measured using KCl denuder is subject to interferences under the conditions of high ozone and relative humidity (Gustin et al., 2012; Huang et al., 2013; Gustin et al., 2015) although it is currently the most accepted method. To evaluate the possible error on interpreting result, K_p was re-calculated with re-calculated GOM concentration using the empirical

322 equation suggested by McClure et al. (2014) (RH=0.63 GOM loss % + 18.1). Since McClure et al.
323 (2014) suggested this equation at RH of 21 to 62%, the GOM concentrations collected only when RH
324 was from 20% to 65% were re-calculated. The multi-linear relationship was compared between re-
325 calculated K_p and original K_p, and the results were very similar to each other (Fig. 2S).
326
327 **3.2. Tracing sources of Hg species**
328 Correlations between Hg and other pollutant concentrations are often used to identify sources. For
329 example good correlations with SO_2 and CO typically indicate the impact of coal combustion (Pirrone
330 et al., 1996; Han et al., 2014), and a strong correlation between Hg and CO has often been used as an
331 indicator for regional transport because both pollutants have similar sources and do not easily
332 decompose by reaction and undergo deposition during transport (Weiss-Penzias et al., 2003, 2006;
333 Kim et al., 2009) although a few recent studies showed the significant bromine-induced oxidation of
334 GEM in the mid-latitude marine boundary layer as well as in the polar atmosphere (Ariya, 201; Obrist
335 et al., 2011) . A good correlation between Hg and NO_2 suggests the site is being impacted by local
336 sources because the lifetime of NO_2 is relatively short compared with that of CO (Seinfeld and Pandis,
337 2006). In this study TGM concentrations were well correlated with SO_2, CO, and PM_{10} concentrations
338 but not with NO_2 concentrations (Table 3), indicating that regional transport of TGM emitted from
339 coal combustion was impacting the site throughout much of the sampling period. PBM concentrations
340 also had a statistically significant relationship with TGM and CO suggesting regional transport is also
341 important for PBM, but GOM was not correlated with any other pollutant suggesting it is impacted to
342 a greater extend by local sources (see additional discussion below).
343 CPF plot shows that the top 25% TGM concentrations were associated with winds from the NNW
344 and eastern direction, pointing towards northeastern China and inland Korean sources; however, when
345 the criterion was set to the top 10% the winds from NNW became less important and the sources
346 located in southern and eastern areas from the sampling site were identified as an important source
347 direction (Fig. 5). The CPF plot for GOM is significantly different from the one for PBM. High PBM
348 concentrations were associated with northern winds while GOM concentrations were enhanced during

349 southeastern winds.

350 These results suggest that for PBM regional transport from Chinese and North Korea sources were
351 more important than Korean sources; in contrast coal fired power plants located in the southern
352 direction rather than regional transport impacted GOM concentration. It should be noted that this
353 result is in apparent conflict with the finding that there was no relationship between GOM and SO_2
354 concentrations. Total SO_2 emissions from power plants in China (18.6 Tg yr^{-1}) are much larger than in
355 Korea (0.09 Tg yr^{-1}), and SO_2 emission rates per capita and per area in China also greatly surpass
356 those in Korea (Lu et al., 2010). Much larger SO_2 emissions in China raise the background SO_2
357 concentration in the region and may mask any correlation between GOM and SO_2 even if coal fired
358 power plants located in the southerly direction from the sampling site impacted GOM concentrations.
359 In support of this hypothesis the pollution rose indicates that high SO_2 concentrations are associated
360 with westerly winds while high GOM concentrations are associated with southerly winds. It should be
361 noted that only the top 25% of GOM and PBM concentrations were used as the criteria for the CPF
362 plot because the number of samples for both species were significantly less than for TGM due to their
363 longer sampling duration (12hr).

364 Among the eight sampling periods, the second period (April, 2013) had the highest TGM, PBM and
365 the second highest GOM average concentration, and SO_2, NO_2, CO, and PM10 were also quite high
366 (Table 1). During this period, TGM was statistically well correlated with SO_2 (r= 0.55), NO_2 (r=0.56),
367 and CO (r=0.36), with the highest Pearson correlation coefficient with NO_2, the characteristic local
368 pollutant. In addition, the CPF plot (for TGM) and the back-trajectories were also associated with
369 easterly winds transporting air masses from major Korean urban areas, supporting the previous
370 suggestion that inland sources enhanced all three Hg concentrations during the second sampling
371 period.

372 In contrast the fifth sampling period had the lowest GOM, PBM and the second lowest TGM
373 concentrations (Table 1). Note however that the TGM concentrations for the first couple of days
374 reached approximately 5 ng m^{-3} and gradually decreased to about 1 ng m^{-3} during the last days of
375 sampling (Fig. 2), indicating that there was likely two different sources affecting Hg concentrations

during this period. Back-trajectories associated with high TGM concentrations passed through northeastern China, North Korea and the industrial/metropolitan areas of Korea before arriving at the sampling site whereas trajectories during the low TGM concentrations spent long periods within the ocean boundary layer. Although Hg can be emitted from ocean surface (Han et al., 2007; UNEP, 2013) heavy rain and low solar radiation occurring during the last two days of this period probably inhibited emissions of Hg from the ocean surface.

3.2.1 GOM/PBM ratio

According to the CPF results, the winds from NW and NE of the sampling site were responsible for the elevated PBM concentrations while easterly winds pointing towards inland Korea were associated with increased GOM concentrations (Fig. 5). The finding that regional transport of TGM and PBM to the site is important is supported by their significant correlation with CO (Table 3). In order to identify the relative importance of local sources relative to regional transport, the ratio of GOM/PBM was used as an indicator because the atmospheric residence time of GOM is widely regarded to be shorter than that of PBM (even though there is no consensus on what specific chemical forms are collected by KCl-coated denuders). The GOM/PBM ratio should be higher if local sources are more important, and the GOM/PBM ratio is likely to decrease as regional transport becomes more important. In this study the GOM/PBM ratios were categorized into three groups: low (0~2), middle (2~8), and high (>8) and the frequency of wind direction was compared (Fig. 6). The result clearly indicates that the southerly and southeasterly winds were associated with high GOM/PBM ratios and that the westerly and northerly winds indicative of regional transport from China prevailed at lower GOM/PBM ratios. There was a weak negative correlation between the ratio of GOM/PBM and CO concentration at a significance level of 0.1 (p-value= 0.089) (Fig. S3), supporting the assertion that the GOM/PBM ratio decreased with the increased effect of regional transport. Lynam and Keeler (2005) also found that high GOM/PBM ratio was observed with influences from local sources and low GOM/PBM ratios appeared with influence from regional sources in Detroit. In Korea, Kim et al. (2009) found a significant increase in the PBM/GOM ratio during high PM2.5 concentration events

caused by regional transport from China.

The reciprocal of this ratio (i.e. GOM/PBM) was used to calculate K_p which indicates that the secondary formation of PBM through gas-particle partitioning was became more important as the significance of regional transport increased, suggesting that secondary production was favored when air underwent regional transport, as has been shown previously (Lynam and Keeler, 2005).

3.2.2 PSCF results

In order to locate potential source areas in more detail, PSCF was used. For TGM, potential sources were located in Liaoning, Shandong, and Henan provinces of China along with the southern area of Korea (Fig. 7). Liaoning province, where large non-ferrous smelters are situated, is the province with the largest Hg emissions in China; Shandong and Henan provinces are also large Hg emission areas, emitting about 30-40 ton yr^{-1} (Fu et al., 2012) in part due to a large lead smelter (Wang et al, 2014), and biomass burning (Huang et al., 2011).

The probable source areas of PBM identified by PSCF were similar to those for TGM, indicating that both Chinese and inland Korean sources enhanced PBM concentrations, with the exception of metropolitan (Seoul) and industrial (Incheon) areas located in northwestern South Korea which emerged as more prominent source areas for PBM than for TGM (Fig. 7). Only Korean sources including metropolitan (Seoul) and the industrial areas in southern Korea were identified as probable source areas for GOM (Fig. 7); regional transport of GOM from China was not important. The Yellow Sea between China and Korea was also associated with high PSCF values, possibly indicating the shipping ports located on the western coast of Korea as important source areas. However, it should be noted that it might be a trailing effect derived by relatively short sampling duration. A trailing effect is often observed, especially with a limited number of measurements or short sampling period, since PSCF evenly distributes weight along the path of trajectories so that PSCF results often identify areas upwind and downwind of real sources as a source area (Han et al., 2007). However, it should be also noted that the marine boundary layer provides good conditions for active Hg oxidation reactions due to an abundance of oxidants (Auzmendi-Murua et al., 2014); therefore, the possibility of areas over

the ocean being a GOM source should not be excluded.

3.2.3 Source attribution based on cluster analysis

In an effort to quantify the contribution of national and foreign sources to the measured Hg concentrations the back trajectories were grouped into five clusters using the trajectory cluster analysis feature of HYSPLIT. Among the five clusters, clusters 1 and 5 represent trajectories originating from outside (South) Korea whereas the trajectories grouped in the cluster 4 originated and passed through the (South) Korean peninsula (Fig. 8). Clusters 2 and 3 contain trajectories from China and the Korean peninsula, but cluster 2 was more associated with Liaoning province and North Korea while cluster 3 originated more from Shandong and Henan provinces. Clusters 1 through 5 contributed 12%, 31%, 26%, 20%, and 11% of the total time, respectively, and the associated concentrations with each cluster are shown in Table 4. Concentration ranges of three Hg species for each cluster were shown as the box-and-whisker plots in the supplementary file (Fig. 5S). When considering that cluster 4 is associated with the local transport from inland Korea and the cluster 1 and 5 are associated with the regional transport from outside of (South) Korea, the maximum and 75th percentile values as well as the arithmetic average are higher in cluster 4 for GOM and PBM than those in the clusters 1 and 5 (Fig. 5S).

The TGM concentration was the highest for cluster 5; however, GOM and PBM concentrations had the lowest averages for this cluster. Cluster 5 contains the back-trajectories originating from Mongolia and Russia and passing through northeastern China before arriving at the sampling site, which suggests regional transport was important for this cluster (Fig. 8). Average CO concentrations were pretty similar for all clusters, but it was the second highest for cluster 5 (cluster 2 was highest). The highest total average GOM and PBM concentrations were associated with cluster 4 which includes trajectories distributed over the Korean peninsula, suggesting that Korean sources were responsible for the enhanced GOM and PBM concentrations. For cluster 4, the highest Pearson correlation coefficient between GOM and PBM concentrations (r=0.721) was observed, indicating that both Hg species were emitted from similar sources. For other clusters, there were no statistically significant

457 correlations between GOM and PBM except for cluster 2 (r=0.209, p-value<0.001). In addition, both
458 average NO_2 concentration (19.4 ±14.9 ppb) and the correlation coefficient between NO_2 and TGM
459 (r= 0.688) were the highest for cluster 4, supporting the finding of impact from Korean sources.
460 In order to consider both Hg concentration and the fraction of time for each cluster, the following
461 equation was used to quantify the effect of Korean and out-of- Korean sources to the Hg concentration
462 at the receptor site.

463 $$\text{source contribution of cluster, i} = \frac{(\frac{N_i}{N_{total}})\times C_j}{\sum_{i=1}^{n}\left\{(\frac{N_i}{N_{total}})\times C_j\right\}} \quad \text{(Eq.6)}$$

464 where (N_i/N_{total}) indicates the percentage of time associated with the cluster, *i*, *i* is the cluster number,
465 *n* is the number of clusters (equal to five in this study), and C_j indicates the average Hg concentration
466 associated with the cluster, *i*. Compared to the other clusters, the source contributions of clusters 1 and
467 4, which represent regional transport, were relatively low for all Hg species (Table 4). Cluster 5
468 contributed more significantly, especially for GOM and PBM, indicating the importance of Korean
469 sources. The source contribution of cluster 2 was the highest for PBM compared to other Hg species,
470 suggesting that North Korean sources were an important contributor to the high PBM concentrations
471 measured, likely due to coal and biomass burning in North Korea (Kim et al., 2013; NI, 2001; NI,
472 2003).
473 In order to quantify the contribution of Korean vs. out-of-Korean sources (note that "Korean"
474 means "South Korean" throughout the manuscript), the source contributions of the clusters were used.
475 Clusters 1 and 5 were used to represent the effect of sources outside of Korea and the cluster 4 was
476 used to indicate the effect of sources in Korea. Since clusters 2 and 3 contain mixed trajectories from
477 Korea and out-of-Korea their contribution was divided evenly between in and out of Korea. The
478 results indicate that the sources in Korea and outside Korea contributed about 50% each to the
479 concentration variation of TGM measured at the sample site during the sampling period while the
480 Korean sources affected GOM and PBM more significantly, accounting for approximately 52.3% and
481 53.4%, respectively (Table 4). These results augment the CPF and PSCF results which only use
482 concentrations that are in the top 25th percentile. While CPF and PSCF found that for high

concentration events Korean sources were most important for GOM while for TGM and PBM regional transport from China and North Korea were also important, the cluster based approach suggests that for all 3 species Korean and out-of-Korean sources contributed approximately 50% each to the concentration variations seen by the site. When the geometric mean concentrations were used for each cluster a similar result was obtained for relative contributions as the results using arithmetic mean concentrations.

It should be noted that errors always exist in calculating trajectories, causing uncertainties in all trajectory-based approaches. Trajectory errors vary considerably from case to case; Stohl (1998) suggested uncertainties might be 20% of the distance travelled by trajectories while Draxler (1996) found that the final error was about 10% of the travel distance.

4. Conclusion and Implications

This study was initiated to identify the sources affecting speciated mercury concentrations measured on an island located between mainland Korea and Eastern China. Various tools were used to locate and quantify the sources, including correlations with other pollutants, CPF, and the back-trajectory based analysis (PSCF and cluster analysis). The results consistently show that Korean sources are most important for GOM while for other Hg species (TGM and PBM) regional transport from China and North Korea were also important. Existing methods including PSCF and CPF are able to locate the source direction and areas, but do not consider the frequency of the wind directions which can affect the long-term concentrations at the receptor site. For example, if the Hg concentration is high with easterly winds both CPF and PSCF identify the eastern areas as important source areas even if, in fact, winds are rarely blowing from east. In this work, it is true that sources located in the eastern direction from the sampling site are likely to be important for enhancing Hg concentrations, but based only on CPF and PSCF results it cannot be said that their contribution to the concentration variations at the site is also high.

Do address this problem a new approach that considers both the cluster frequency and the Hg concentration associated with each cluster was used to quantify the source contribution at the

sampling site. On average, contributions from out-of-Korean sources were similar to Korean sources for TGM whereas Korean sources contributed slightly more to the concentration variations of GOM and PBM compared to the out-of-Korean sources. However uncertainties exist in the source attribution approach based on cluster analysis because the trajectories inevitably overlap between different clusters since the cluster analysis accounts for both variations in transport speed and direction simultaneously. However, this new approach can augment the existing methods including CPF and PSCF to help identify source contributions to the concentration variations at the sampling site.

The ratio of GOM/PBM proved to be a useful tool for identifying the relative significance of local sources vs. regional transport. The GOM/PBM ratio decreased as the effect of regional transport increased and vice versa since GOM has a shorter atmospheric residence time than PBM. The K_p calculated using the reciprocal of the GOM/PBM ratio was negatively correlated with atmospheric temperature and positively correlated with relative humidity, suggesting that the secondary formation of PBM was an important source of atmospheric PBM concentration at low temperature and high relative humidity. This result also suggests that the secondary formation of PBM becomes more favored when the air undergoes regional transport rather than local transport.

Acknowledgements

This work was funded by the National Research Foundation of Korea (NRF) grant funded by the Korea government (MSIP) (No. 2015R1A2A2A03008301) and the Korea Ministry of Environment (MOE) as “the Environmental Health Action Program”. This research was also supported by 2014 Research Grant from Kangwon National University (No. C1011758-01-01).

Author Contributions

The work presented here was carried out in collaboration between all authors. Gang S. Lee analyzed data and wrote the paper. Pyung R. Kim performed the experiments and interpreted the results. Young J. Han defined the research theme, interpreted the results, and wrote the paper. Yong S. Seo, Seung.

M. Yi, and Thomas M. Holsen also interpreted the results and approved the final paper.

Conflicts of Interest

The authors declare no conflict of interest.

Reference

AMAP/UNEP: Technical Background Report on the Global Anthropogenic Mercury Assessment; Arctic Monitoring and Assessment Programme/UNEP Chemicals Branch, p. 159., 2008.

Amato, F. and Hopke, P.K.: Source apportionment of the ambient PM2.5 across St. Louis using constrained positive matrix factorization, Atmos. Environ., 329-337, 2012.

Amos, H. M., Jacob, D. J., Holmes, C. D., Fisher, J. A., Wang, Q., Yantosca, R. M., Corbitt, E. S., Galarneau, E., Rutter, A. P., Gustin, M. S., Steffen, A., Schauer, J. J., Graydon, J. A., St Louis, V. L., Talbot, R. W., Edgerton, E. S., Zhang, Y., and Sunderland, E. M.: Gas-particle partitioning of atmospheric Hg(II) and its effect on global mercury deposition, Atmos, Chem. Phys., 12, 591–603, 2012.

Ariya, P.A.: Atmospheric science: mid-latitude mercury loss, Nature Geoscience, 4, 14-15, 2011.

Auzmendi-Murua, I., Castillo, A. and Bozzelli J.W.: Mercury Oxidation via Chlorine, Bromine, and Iodine under atmospheric conditions: Thermochemistry and Kinetics, J. Phy. Chem., 118, 2959-2975, 2014.

Baya, A.P. and Van Heyst, B.: Assessing the trends and effects of environmental parameters on the behaviour of mercury in the lower atmosphere over cropped land over four season, Atmos. Chem. Phys., 10, 8617-8628, doi:10.5194/acp-10-8617-2010, 2010.

564

565 Cheng, I., Zhang, L., Mao, H., Blanchard, P., Tordon, R. and John, D.: Seasonal and diurnal patterns
566 of speciated atmospheric mercury at a coastal-rural and coastal-urban site, Atmos. Environ., 82, 193–
567 205, 2014.

568

569 Choi, H. D., Holsen, T. M. and Hopke, P. K.: Atmospheric mercury in the Adirondacks:
570 concentrations and sources, Environ. Sci. Technol., 42, 5644-5653, 2008.

571

572 Draxler, R.R.: Trajectory optimization for balloon flight planning, Weather and Forecasting, 11, 111-
573 1114, 1996.

574

575 Draxler, R.R., Stunder, B., Rolph, G., Stein, A. and Taylor, A.: HYSPLIT_4 User's Guide. Silver
576 Spring, Maryland, USA: NOAA Air Resour. Lab., Available at
577 http://www.arl.noaa.gov/documents/reports/hysplit_user_guide.pdf, 2014.

578

579 Driscoll, C.T., Han, Y.J., Chen, C.Y., Evers, D.C., Lambert, K.F., Holsen, T.M., Kamman, N.C. and
580 Munson, R.K.: Mercury contamination in forest and freshwater ecosystems in the Northeastern United
581 States, Bioscience, 57, 17–28, 2007.

582

583 Edgerton, E.S., personal communication.

584

585 Fang, G.C., Zhang, L. and Huang, C.S.: Measurement of size-fractionated concentration and bulk dry
586 deposition of atmospheric particulate bound mercury, Atmos. Environ., 61, 371–377, 2012.

587

588 Feng, X., Lu, J.Y., Conrad, D.G., Hao, Y., Banic, C.M. and Schroeder, W.H.: Analysis of inorganic
589 mercury species associated with airborne particulate matter/aerosols: method development, Anal.
590 Bioanal. Chem., 380, 683-689, 2004

Finley, B.D., Jaffe, D.A., Call, K., Lyman, S., Gustin, M.S., Peterson, C., Miller, M. and Lyman, T.: Development, testing, and deployment of an air sampling manifold for spiking elemental and oxidized mercury during the Reno atmospheric mercury intercomparison experiment (RAMIX). Environ. Sci. Technol. 47(13), 7277-7284, 2013.

Fu, X., Feng, X., Qiu, G., Shang, L. and Zhang, H.: Speciated atmospheric mercury and its potential source in Guiyang, China, Atmos. Environ., 45, 4205–4212, 2011.

Galindo, N., Yubero, E., Nicolás, J.F., Crespo, J., Pastor, C., Carratalá, A., and Santacatalina, M.: Water-soluble ions measured in fine particulate matter next to cement works, Atmos. Environ., 45, 2043-2049, 2011.

Gratz, L.E., Keeler, G.J., Marsik, F.J., Barres, J.A., Dvonch, T.: Atmospheric transport of speciated mercury across southern Lake Michigan: Influence from emission sources in the Chicago/Gary urban area, Sci. Total Environ., 448, 84-95, 2013.

Gustin, M.S., Huang, J., Miller, M.B., Peterson, C., Jaffe, D.A., Ambrose, J., Finley, B.D., Lyman, S.N., Call, K., Talbot, R., Feddersen, D.,, Mao, H. and Lindberg, S.E.: Do we understand what the mercury speciation instruments are actually measuring? Results of RAMIX. Environ. Sci. Technol. 47(13), 7295-7306, 2013.

Gustin, M.S., Amos, H.M., Huang, J., Miller, M.B., and Heidecorn, K.; Measuring and modeling mercury in the atmosphere: a critical review, Atmos. Chem. Phys., 15, 5697-5713, 2015.

Han, Y.J., Holsen, T.M. and Hopke, P.K.: Estimation of source location of total gaseous mercury measured in New York State using trajectory-based models, Atmos. Environ., 41, 6033–6047, 2007.

618

619 Han, Y. J., Kim, J. E., Kim, P. R., Kim, W. J., Yi, S. M., Seo, Y. S. and Kim, S. H.: General trends of
620 Atmospheric mercury concentrations in urban and rural areas in Korea and characteristics of high-
621 concentration events, Atmos. Environ., 94, 754-764, 2014.

622

623 Hedgecock, I. M. and Pirrone, N.: Chasing quicksilver: Modeling the atmospheric lifetime of Hg0 (g)
624 in the marine boundary layer at various latitudes, Environ. Sci. Technol., 38(1), 69-76, 2004.

625

626 Huang, J., Choi, H.D., Hopke, P.K. and Holsen, T.M.: Ambient mercury sources in Rochester, NY :
627 Results from principal components analysis (PCA) of mercury monitoring network data. Environ. Sci.
628 Technol., 44, 8441-8445, 2010.

629

630 Huang, X., Li, M., Friedli, H. R., Song, Y., Chang, D. and Zhu, L.: Mercury Emissions from Biomass
631 Burning in China. Environ, Sci. Technol., 45, 9442-9448, 2011.
632 Huang, J. and Gustin, M.S.: Evidence for a free troposphere source of mercury in wet deposition in
633 the Western United States, Environ. Sci. Technol., 46(12), 6621-6629, 2012.

634

635 Huang, J., Miller, M.B., Weiss-Penzias, P. and Gustin, M.S.: Comparison of gaseous oxidized Hg
636 measured by KCl-coated denuders, and nylon and cation exchange membranes. Environ. Sci. Technol.,
637 47(13), 7307-7316, 2013.

638

639 IEA, International Energy Agency :
640 http://www.iea.org/stats/countryresults.asp.COUNTRY_CODE=KP&Submit=Submit: 2012.

641

642 Jaffe, D.A., Lyman, S., Amos, H.M., Gustin, M.S., Huang, J., Selin, N.E., Levin, L., Sschure, A.T.,
643 Mason, R.P., Talbot, R., Rutter, A., Finley,, B., Jaeglé, L., Shah, V., McClure, C., Ambrose, J., Gratz,
644 L., Lindberg, S., Weiss-Penzias, P., Sheu, G.R., Fedddersen, DD., Horvat, M., Dastoor, A., Hynes, A.J.,

Mao, H., Sonke, J.E., Slemr, F., Fisher, J.A., Ebinghaus, R., Zhang, Y. and Edwards, G.: Progress on understanding atmospheric mercury hampered by uncertain measurements, Environ. Sci. Technol., 48, 7204-7206, 2014.

Kelly, C., Toro, R., Di Martino, A., Cox, C.L., Bellec, P., Castellanos, F.X., and Milham, M.P.: A convergent functional architecture of the insula emerges across imaging modalities, Neuroimage, 61, 1129-1142, 2012.

Kim, J.H., Park, J.M., Lee, S.B., Pudasainee, D. and Seo, Y.C.: Anthropogenic mercury emission inventory with emission factors and total emission in Korea, Atmos. Environ., 44, 2714-2721, 2010.

Kim, M., Deshpande, S.R, Crist, K.C.: Source apportionment of fine particulate matter (PM2.5) at a rural Ohio River Valley site, Atmos. Environ., 41, 9231-9243, 2007.

Kim, I.S., Lee, J.Y., and Kim, Y.P.: Impact of polycyclic aromatic hydrocarbon (PAH) emissions from North Korea to the air quality in the Seoul Metropolitan Area, South Korea, Atmos. Environ., 70, 159-165, 2013.

Kim, P. R., Han, Y.J., Holsen, T.M. and Yi, S.M.: Atmospheric particulate mercury: Concentrations and size distributions, Atmos. Environ., 61, 94-102, 2012.

Kim, S.H., Han, Y.J., Holsen, T.M. and Yi, S.M.: Characteristics of atmospheric speciated mercury concentrtions (TGM, Hg(Ⅱ), and Hg(p)) in Seoul, Korea, Atmos. Environ., 43, 3267-3274, 2009.

Lan, X., Talbot, R., Castro, M., Perry, K. and Luke, W.: Seasonal and Diurnal Variations of Atmospheric Mercury across the US Determined from AMNet Monitoring Data, Atmos. Chem. Phys., 12, 10569–10582, 2012.

672
673 Landis, M.S. and Keeler, G.J.: Atmospheric mercury deposition to Lake Michigan during the Lake
674 Michigan mass balance study, Environ. Sci. Technol., 36, 4518-4524, 2002
675
676 Lee, G.S., Kim, P.R., Han, Y.J., Holsen, T.M., and Lee, S.H.: Tracing sources of total gaseous mercury
677 to Y ongheung Island off the coast of Korea, Atmosphere, 5, 273-291, 2014.
678
679 Lin, C. J. and Pehkonen, S. O.: The chemistry of atmospheric mercury: a review, Atmos. Environ.,
680 33(13), 20674-2079, 1999.
681
682 Lyman, S.N. and Gustin, M.S.: Determinants of atmospheric mercury concentrations in Reno, Nevada,
683 USA. Sci. Total. Environ., 408, 431-438, 2009.
684
685 Lyman, S.N.; Jaffe, D.A. and Gustin, M.S.: Release of mercury halides from KCl denuders in the
686 presence of ozone. Atmos. Chem. Phys. 10(17), 8197-8204, 2010.
687
688 Lynam, M. M. and Keeler, G. J.: Automated speciated mercury measurements in Michigan, Environ.
689 Sci. Technol., 39, 9253-9562, 2005.
690
691 Liu, B., Keeler, G.J., Timothy Dvonch, J., Barres, J.A., Lynam, M.M., Marsik, F.J. and Morgan, J.T.:
692 Urban-rural differences in atmospheric mercury speciation, Atmos. Environ., 44, 2013-2023, 2010.
693
694 Lu, W., Zhu, Z.Y. and Liu, W.P.: Salt water intrusion numerical simulation on application based on
695 FEFLOW, Ground Water, 32, 19–21, 2010.
696
697 McClure, C.D., Jaffe, D.A. and Edgerton, E.S.: Evaluation of the KCl denuder method for gaseous
698 oxidized mercury using HgBr2 at an In-Service AMNet site, Environ. Sci. Technol., 48, 11437-11444,

2014.

Malcolm, E.G. and Keeler, G.J.: Evidence for a sampling artifact for particulate-phase mercury in the marine atmosphere, Atmos. Environ. 41(16), 3352-3359, 2007.

Mao, H., Talbot, R., Hegarty, J., and Koermer, J.: Speciated mercury at marine, coastal, and inland sites in New England Part 2: Relationships with atmospheric physical parameters, Atmos. Chem. Phys., 12, 4181-4206, 2012.

Mason, R.P., Morel, F.M.M. and Hemond, H.F.: The role of microorganisms in elemental mercury formation in natural water, Water Air Soil Poll, 80, 775-787, 1995.

Mason, R.P. and Sullivan, K.A.: Mercury in Lake Michigan, Environ. Sci. Technol., 31, 942-947, 1997.

Mergler, D., Anderson, H.A., Chan, L.H.M., Mahaffey, K.R., Murray, M., and Sakamoto, M.: Methylmercury exposure and health effects in humans: a worldwide concern, Ambio 36:3-11, 2007.

NI, Nautilus Institute for Security and Sustainable Development: Rural energy survey in U nhari Village, the Democratic People's Republic of Korea (DPRK): Methods, results, and implications, Berkely, California, USA, 2001.

NI, Nautilus Institute for Security and Sustainable Development: The DPRK Energy Sector: Estimated Year 2000 Energy Balance and Suggested Approaches to Sectoral Redevelopment, Berkeley, California, USA, 2003

Obrist, D., Johnson, D. W., Lindberg, S. E., Luo, Y., Hararuk, O., Bracho, R., Battles, J. J., Dail, D. B.,

726 Edmonds, R. L., Monson, R. K., Ollinger, S. V., Pallardy, S. G., Pregitzer, K. S. and Todd D. E.:
727 Mercury Distribution Across 14 U.S. Forests. Part I: Spatial Patterns of Concentrations in Biomass,
728 Litter, and Soils, Environ. Sci. Technol., 45(9), 3974-3981, 2011.
729
730 Pirrone, N., Aas, W., Cinnirella, S., Ebinghaus, R., Hedgecock, I. M., Pacyna, J., Sprovieri, F. and
731 Sunderland, E. M.: Toward the next generation of air quality monitoring: Mercury, Atmos. Environ.,
732 80, 599-611, 2013.
733
734 Pirrone, N., Keeler, G. J. and Nriagu, J. O.: Regional differences in worldwide emissions of mercury
735 to the atmosphere, Atmos. Environ., 30, 2981–2987, 1996.
736
737 Polissar, A.V., Hopke, P.K. and Harris, J.M.: Source regions for atmospheric aerosol measured at
738 Barrow, Alaska, Environ. Sci. Technol., 35, 4214–4226, 2001.
739
740 Polissar, A.V., Hopke, P.K. and Poirot, R.L.: Atmospheric aerosol over Vermont: Chemical
741 composition and sources, Environ. Sci. Technol., 35, 4604–4621, 2001.
742
743 Rutter, A.P. and Schauer, J.J.: The effect of temperature on the gas-particle partitioning of reactive
744 mercury in atmospheric aerosols, Atmos. Environ., 41, 8647-8657, 2007a
745
746 Rutter, A.P. and Schauer, J.J.: The impact of aerosol composition on the particle to gas partitioning of
747 reactive mercury, Environ. Sci. Technol., 41(11), 3934-3939, 2007b
748
749 Seinfeld, J.H. and Pandis, S. N.: Atmospheric chemistry and physics: From air pollution to climate
750 change, second ed. John Wiley & Sons, Inc., Hoboken, New Jersey, USA, 2006.
751
752 Stohl, A.: Computation, accuracy and applications of trajectories- A review and bibliography, Atmos.

753 Environ., 32(6), 947-966, 1998.
754
755 Subir, M., Ariya, P. A., and Dastoor, A. P.: A review of uncertainties in atmospheric modeling of
756 mercury chemistry I. Uncertainties in existing kinetic parameters–Fundamental limitations and the
757 importance of heterogeneous chemistry, Atmos. Environ., 45(32), 5664-5676, 2011.
758
759 Subir, M., Ariya, P. A., and Dastoor, A. P.: A review of the sources of uncertainties in atmospheric
760 mercury modeling II. Mercury surface and heterogeneous chemistry–A missing link, Atmos. Environ.,
761 46, 1-10, 2012.
762
763 Talbot, R., Mao, H., Feddersen, D., Smith, M., Kim, S.Y., Sive, B., Haase, K., Ambrose, J., Zhou, Y.
764 and Russo, R.: Comparison of particulate mercury measured with manual and automated methods,
765 Atmosphere, 2, 1-20, 2011.
766
767 Temme, C., Einax, Jr.., W., Ebinghaus, R., and Schroeder, W.H.: Measurements of atmospheric
768 mercury species at a coastal site in the Antarctic and over the South Atlantic Ocean during polar
769 summer, Environ. Sci. Technol., 37, 22-31, 2002
770
771 Timonen, H., Ambrose, J.L., Jaffe, D.A.: Oxidation of elemental Hg in anthropogenic and marine
772 airmasses, Atmos. Chem. Phys., 13, 2827-2836, 2013.
773
774 U.S. EPA,: Mercury Study Report to Congress. Office of Air Quality Planning and Standards and
775 Office of Research and Development, EPA-452/R-97-005, 1997.
776
777 UNEP.: The Global Atmospheric Mercury Assessment; UNEP Chemicals Branch: Geneva,
778 Switzerland, 2013.
779

780 Wan, Q., Feng, X.B., Julia, L., Zheng, W., Song, X.J., Han, S.J.,, and Xu, H.: Atmospheric mercury in
781 Changbai Mountain area, northeastern China – Part 1: The seasonal distribution pattern of total
782 gaseous mercury and its potential sources, Environ. Res., 109, 201-206, 2009a
783
784 Wan, Q., Feng, X.B., Julia, L., Zheng, W., Song, X.J., Han, S.J.,, and Xu, H.: Atmospheric mercury in
785 Changbai Mountain area, northeastern China II. The distribution of reactive gaseous mercury and
786 particulate mercury and mercury deposition fluxes, Environ. Res., 109, 721-727, 2009b
787
788 Wang, L., Wang, S., Zhang, L., Wang, Y., Zhang, Y., Nielsen, C., McElroy, B. M. and Hao, J.: Source
789 apportionment of atmospheric mercury pollution in China using the GEOS-Chem model, Environ.
790 Poll., 190, 166-175, 2014.
791
792 Wang, S., Holsen, T.M., Huang, J. and Han, Y.J.: Evaluation of various methods to measure
793 particulate bound mercury and associated artifacts, Atmos. Chem. Phys. Discuss. 13, 8585-8614, 2013.
794
795 Weiss-Penzias, P., Jaffe, D.A., Mcclintick, A., Prestbo, E.M. and Landis, M.S.: Gaseous elemental
796 mercury in the marine boundary layer: evidence for rapid removal in anthropogenic pollution,
797 Environ. Sci. Technol., 37, 3755-3763, 2003.
798
799 Weiss-Penzias, P., Jaffe, D.A., Swartzendruber, P., Dennison, J.B., Chand, D., Hafner, W. and Prestbo,
800 E.,: Observations of Asian air pollution in the free troposphere at Mount Bachelor Observatory during
801 the spring of 2004, J. Geophys. Res., 111 (D10304), 1-15, 2006.
802
803 Weiss-Penzias, P., Gustine, M.S., Lyman, S.: Observations of speciated atmospheric mercury at three
804 sites in Nevada, USA: Evidence for a free tropospheric source of reactive gaseous mercury, J. of
805 Geophys. Res., 114, D14302, doi:10.1029/2008JD011607, 2009
806

Xiu, G.L., Jin, Q.X., Zhang, D.N., Shi, S.Y., Huang, X.J., Zhang, W.Y., Bao, L., Gao, P.T. and Chen, B.: Characterization of size-fractionated Particulate Mercury in Shanghai Ambient Air. Atmos, Environ., 39, 419–427, 2005.

Xiu, G.L., Cai, J., Zhang, W.Y., Zhang, D.N., Bueler, A., Lee, S.C., Shen, Y., Xu, L.H., Huang, X.J. and Zhang, P.: Speciated Mercury In size Fractionated Particles in Shanghai Ambient Air, Atmos. Environ., 43, 3145–3154, 2009.

Xu, L.L., Chen, J.S., Yang, L.M., Niu, Z.C., Tong, L., Yin, L.Q., and Chen, Y.T.: Characteristics and sources of atmospheric mercury speciation in a coastal city, Xiamen, China, Chemosphere, 119, 530-539, 2015.

You, C.H., Kim, B.G., Jo, E.M., Kim, G.Y., Yu, B.C., Hong, M.G., Kim, D.S., and Hong, Y.S.: The relationship between the fish consumption and blood total/methyl-mercury concentration of coastal area in Korea, NeuroToxicology, 33, 676-682, 2012.

Zhang, H., Feng, X., Larseen, T., Qiu, G., and Vogt, R.D.: In inland China, rice, rather than fish, is the major pathway for methylmercury exposure, Environmental Health Perspectives, 118, 1183-1188, 2010.

Zhang, L., Gong, S., Padro, J. and Barrie, L.: A size-segregated particle dry deposition scheme for and atmospheric aerosol module, Atmos. Environ., 35, 549–560, 2001.

Zhang, H., Fu, X.W., Lin, C.-J., Wang, X., and Feng, X.B.: Observation and analysis of speciated atmospheric mercury in Shangri-La, Tibetan Plateau, China, Atmos. Chem. Phys., 15, 653-665, 2015.

Table list

Table 1 Summarized concentrations of speciated Hg and other typical pollutants for each sampling period.

Table 2. Comparisons of measured Hg concentrations with those reported in other studies.

Table 3. Correlation coefficients and p-values (in parenthesis) for speciated Hg with other pollutants for the whole sampling period. Correlation coefficients with an asterisk indicate a statistically significant relationship at $\alpha = 0.05$.

Table 4. Estimated contribution of Korean and out-of-Korean sources on variations of speciated Hg concentration. *: TGM is shown in ng m^{-3} while for both GOM and PBM the units are pg m^{-3}.

Figure list

Figure 1. (a) The sampling site in Yongheung Island (the star mark). (b) Anthropogenic mercury emission sources in Korea. Blue star indicates the sampling site, and the green circle indicates the area where major Korean coal-fired power plants are located. (c) The enlarged image of the area near the sampling site.

Figure 2. TGM, GOM, and PBM concentrations measured during the eight sampling periods. TGM was measured every 5 minutes while GOM and PBM were measured during 12hrs except for the 2hr measurements during May, 2014.

Figure 3. Box-and-whisker plot for the concentrations of TGM, GOM, and PBM during three different periods. The red dash lines indicate the arithmetic mean.

Figure 4. The gas-particle partitioning coefficient, K_p, related to atmospheric temperature and relative humidity (RH) (n=81)..

Figure 5. CPF plots for TGM using the top 25% (left upper panel) and the top 10% (right upper panel) as a criterion, and for GOM (left bottom panel) and for PBM (right bottom panel). For both GOM and PBM, the criterion of the top 25% concentration was used.

Figure 6. Frequency of wind direction with different GOM/PBM ratios. Southerly and easterly winds prevailed for the samples with high GOM/PBM ratio whereas the percentage of westerly winds increased as the GOM/PBM ratio decreased.

Figure 7. PSCF results for TGM (left), PBM (middle), and GOM (right) using the top 25% of concentrations as criteria.

887 Figure 8. Back-trajectories for clusters 1 through 5. The left top panel indicates the mean back-
888 trajectory and contribution for each cluster.

Table 1 Summarized concentrations of speciated Hg and other typical pollutants for each sampling period

Sampling periods	TGM (ng m^{-3})	GOM (pg m^{-3})	PBM (pg m^{-3})	SO_2 (ppb)	NO_2 (ppb)	CO (ppm)	O_3 (ppb)	PM_{10} (μg m^{-3})
1st : 2013.01.17 ~ 01.23	3.5 ± 0.8	5.8 ± 8.8	17.0 ± 16.5	5.8 ± 4.2	26.7 ± 12.4	0.5 ± 0.2	21.7 ± 13.5	55.9 ± 38.5
2nd : 2013.02.25 ~ 03.01	3.7 ± 0.9	13.2 ± 14.8	19.5 ± 19.6	7.3 ± 3.0	28.8 ± 19.1	0.7 ± 0.2	28.3 ± 14.7	83.6 ± 28.6
3rd : 2013.04.08 ~ 04.13	2.1 ± 0.4	4.3 ± 5.6	15.6 ± 13.8	4.9 ± 1.7	8.6 ± 3.3	0.4 ± 0.1	46.8 ± 6.0	45.8 ± 21.4
4th : 2013.05.20 ~ 05.25	2.8 ± 1.0	4.2 ± 5.9	6.7 ± 7.3	5.7 ± 2.5	17.2 ± 5.9	0.5 ± 0.1	36.2 ± 19.4	51.9 ± 21.6
5th : 2013.08.19 ~ 08.24	2.3 ± 0.9	3.2 ± 3.0	5.4 ± 4.6	4.7 ± 1.6	10.2 ± 3.8	0.5 ± 0.1	40.9 ± 29.6	34.2 ± 13.7
6th : 2014.03.17 ~ 03.21	2.6 ± 1.2	12.8 ± 15.7	7.3 ± 3.5	7.5 ± 0.1	32.9 ± 75.1	0.4 ± 0.2	39.0 ± 12.5	66.7 ± 44.4
7th : 2014.05.26 ~ 05.31	2.8 ± 0.7	13.5 ± 9.0	9.8 ± 12.2	5.8 ± 2.3	12.4 ± 5.6	0.5 ± 0.1	85.5 ± 23.3	124.5 ± 44.9
8th : 2014.08.19 ~ 08.23	2.4 ± 1.1	10.7 ± 3.7	6.3 ± 3.6	3.4 ± 1.2	8.7 ± 6.0	0.4 ± 0.1	38.7 ± 16.5	32.0 ± 22.3
Average	2.8 ± 1.1	8.3 ± 9.7	10.9 ± 11.2	5.6 ± 5.0	18.2 ± 28.7	0.5 ± 0.2	42.1 ± 25.8	61.9 ± 42.8

Table 2. Comparisons of measured Hg concentrations with those reported in other studies.

Country	Site	Remarks	Year	TGM (ng m^{-3})	GOM (pg m^{-3})	PBM (pg m^{-3})	Reference
Korea	Seoul	Urban	2005-2006	3.22 ± 2.10	27.2 ± 19.3	23.9 ± 19.6	Kim et al., 2009
	Seoul	Urban	2006-2009	3.72 ± 2.96	11.3 ± 9.5	13.4 ± 12.0	Han et al., 2014
	Chuncheon	Rural	2006-2009	2.12 ± 1.47	2.7 ± 2.7	3.7 ± 5.7	Han et al., 2014
	Yongheung	**Island**	**2013-2014**	**2.8 ± 1.1**	**9.8 ± 9.9**	**10.6 ± 12.0**	**This study**
China	Guiyang	Urban	2009	9.7 ± 10.2	35.7 ± 43.9	368.0 ± 676.0	Fu et al., 2011
	Xiamen	Suburban	2012-2013	3.5	61.05	174.41	Xu et al., 2015
	Mt. Changbai	Remote	2005-2006	3.58 ± 1.78	65 ± 84	77 ± 136	Wan et al., 2009a,b
USA	Chicago	Urban	2007	2.5 ± 1.5	17 ± 87	9 ± 20	Gratz et al., 2013
	Reno, Nevada	Suburban	2007-2009	2.0 ± 0.7	18 ± 22	7 ± 7	Lyman and Gustin, 2009
	Rochester, NY	Urban	2008-2009	1.49	4.08	6.57	Huang et al., 2010
Canada	Nova Scotia	Urban	2010-2011	1.67 ± 1.01	2.07 ± 3.35	2.32 ± 3.09	Cheng et al., 2014
	Ontario	Rural	2006-2007	1.17	15.10	16.40	Baya and Van Heyst, 2010

Table 3. Correlation coefficients and p-values (in parenthesis) for speciated Hg with other pollutants for the whole sampling period. Correlation coefficients with an asterisk indicate a statistically significant relationship at $\alpha = 0.05$.

	TGM	**GOM**	**SO_2**	**NO_2**	**CO**	**O_3**	**PM_{10}**
TGM	-	-0.132 (0.233)	**0.115*** (0.001)	0.063 (0.074)	**0.571*** (<0.001)	-0.055 (0.115)	**0.401****(<0.001)
GOM	-0.132 (0.233)	-	0.025 (0.822)	0.022 (0.846)	-0.149 (0.180)	0.143 (0.197)	0.128 (0.248)
PBM	**0.235*** (0.030)	0.021 (0.855)	-0.006 (0.954)	0.008 (0.941)	**0.215*** (0.048)	0.029 (0.794)	0.139 (0.206)

Table 4. Estimated contribution of Korean and out-of-Korean sources on variations of speciated Hg concentration.
*: TGM is shown in ng m^{-3} while for both GOM and PBM the units are pg m^{-3}.

Cluster	Cluster frequency (%)	Average concentration*			Source contribution (%)			Korean (%)			Out-of-Korean (%)		
		TGM	GOM	PBM	TGM	GOM	PBM	TGM	GOM	PBM	TGM	GOM	PBM
1	12	2.2	6.9	7.7	9.6	10.5	8.6				9.6	10.5	8.6
2	31	2.8	8.3	12.6	31.5	32.5	36.5	15.7	16.3	18.2	15.7	16.3	18.2
3	26	2.9	8.1	10.0	27.3	26.6	24.3	13.7	13.3	12.1	13.7	13.3	12.1
4	20	2.6	9.0	12.3	18.9	22.8	23.0	18.9	22.8	23.0			
5	11	3.2	5.5	7.4	12.8	7.6	7.6				12.8	7.6	7.6
Korean								**48.3**	**52.3**	**53.4**			
Out-of-Korean											**51.7**	**47.7**	**46.6**

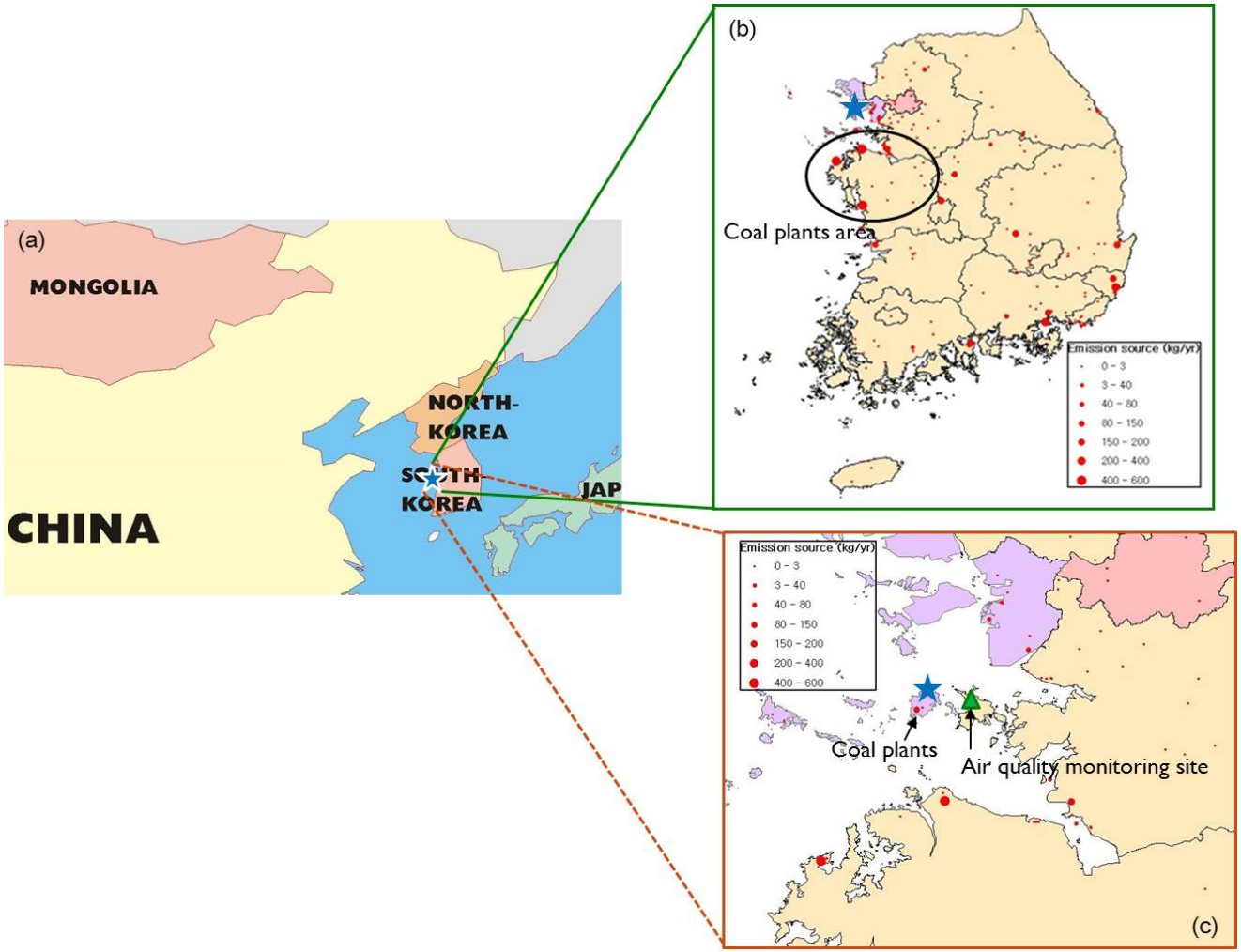

Figure 1. (a) The sampling site in Yongheung Island (the star mark). (b) Anthropogenic mercury emission sources in Korea. Blue star indicates the sampling site, and the green circle indicates the area where major Korean coal-fired power plants are located. (c) The enlarged image of the area near the sampling site.

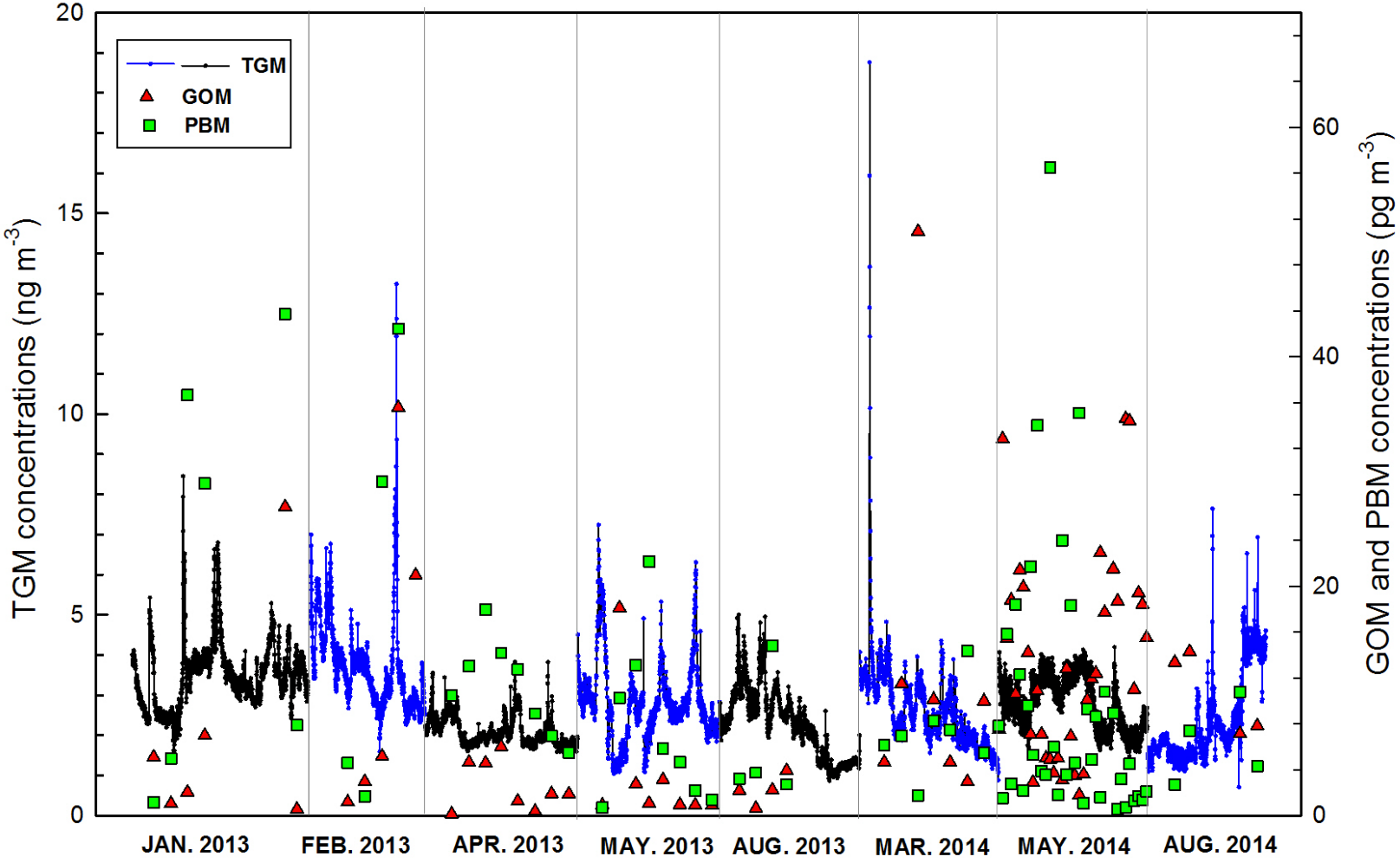

Figure 2. TGM, GOM, and PBM concentrations measured during the eight sampling periods. TGM was measured every 5 minutes while GOM and PBM were measured during 12hrs except for the 2hr measurements during May, 2014.

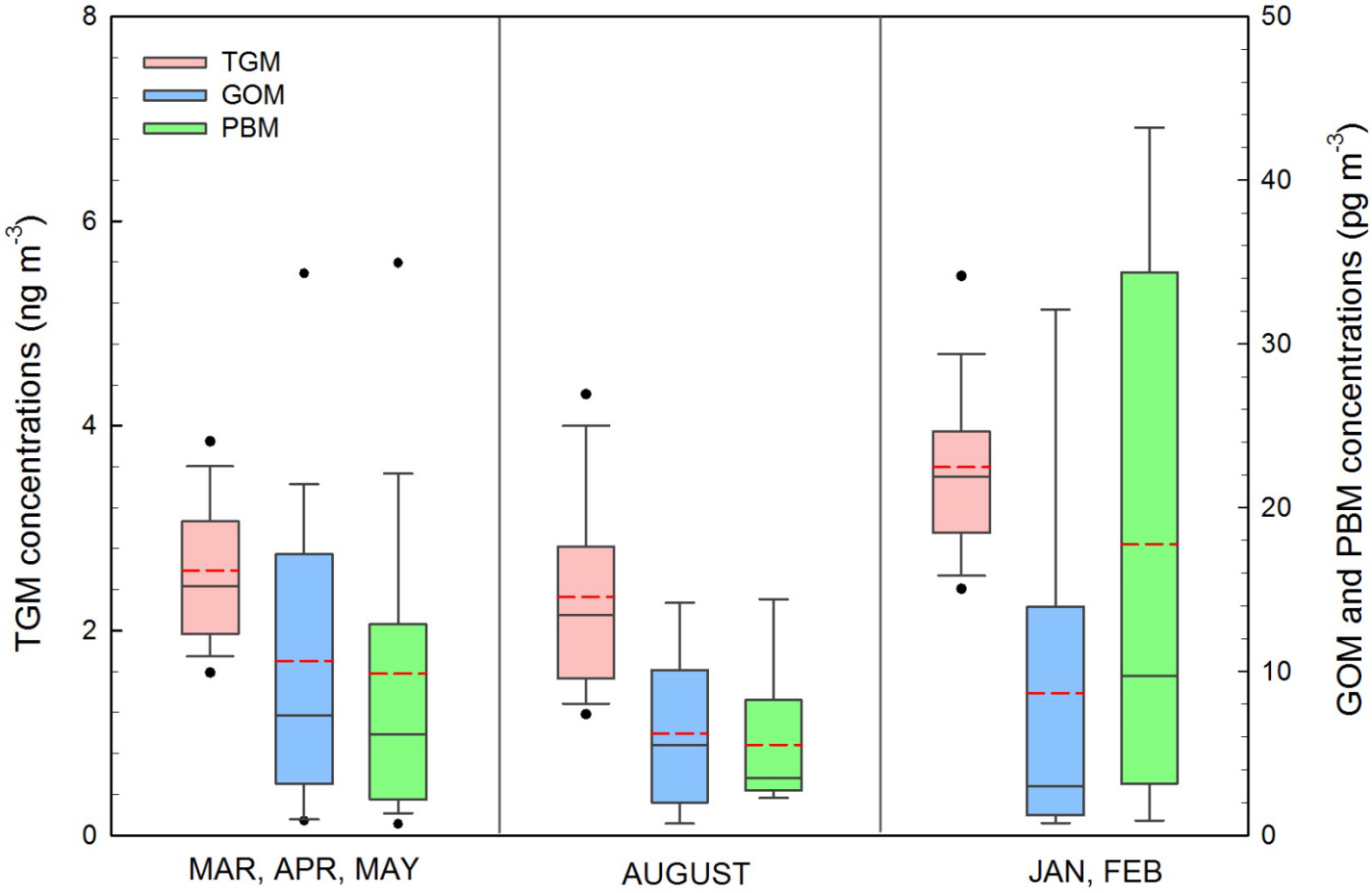

Figure 3. Box-and-whisker plot for the concentrations of TGM, GOM, and PBM during three different periods. The red dash lines indicate the arithmetic mean.

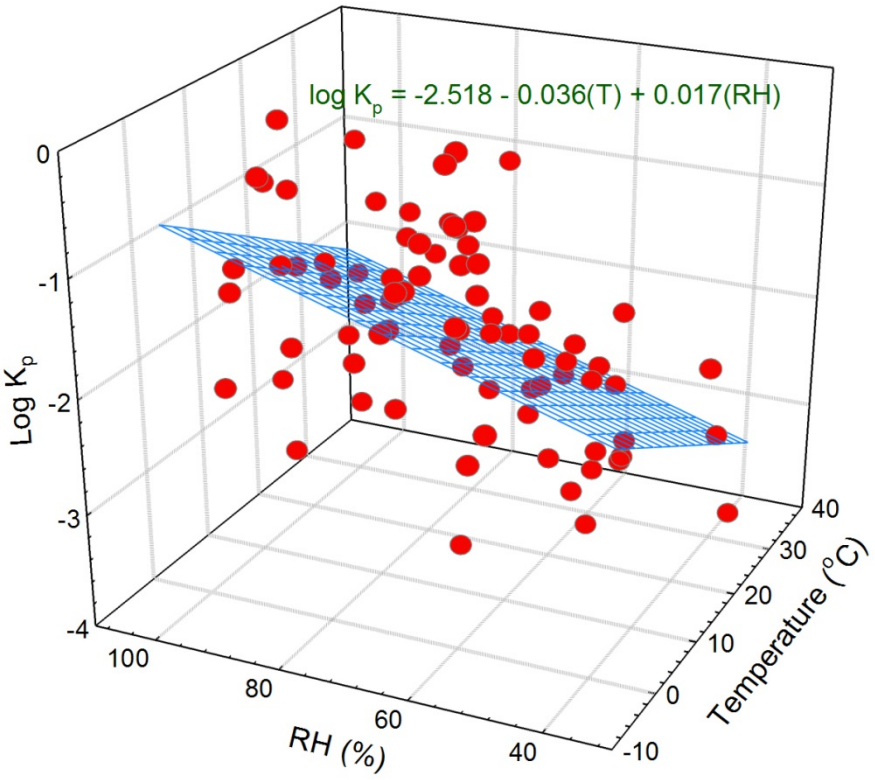

Figure 4. The gas-particle partitioning coefficient, K_p, related to atmospheric temperature and relative humidity (RH) (n=81).

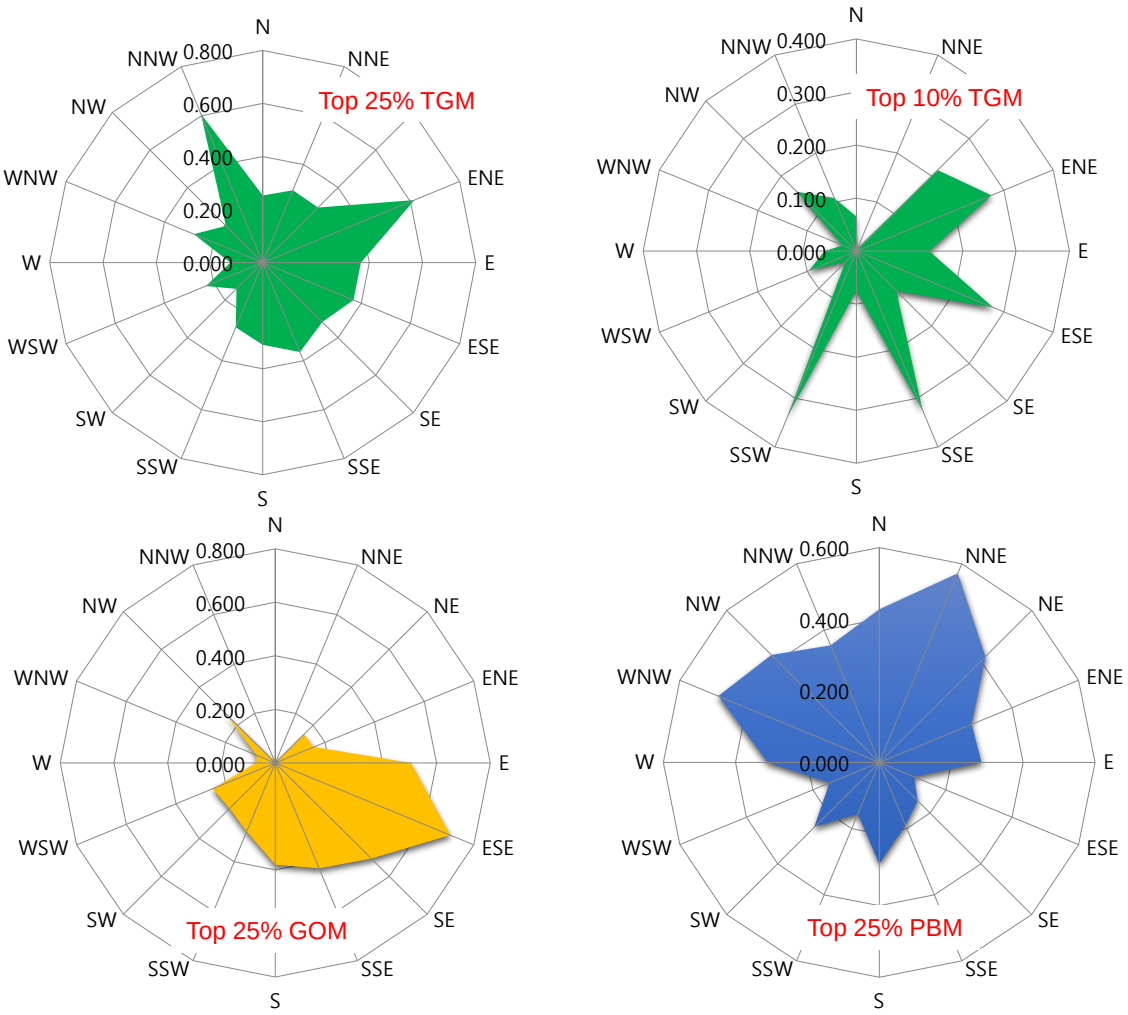

Figure 5. CPF plots for TGM using the top 25% (left upper panel) and the top 10% (right upper panel) as a criterion, and for GOM (left bottom panel) and for PBM (right bottom panel). For both GOM and PBM, the criterion of the top 25% concentration was used.

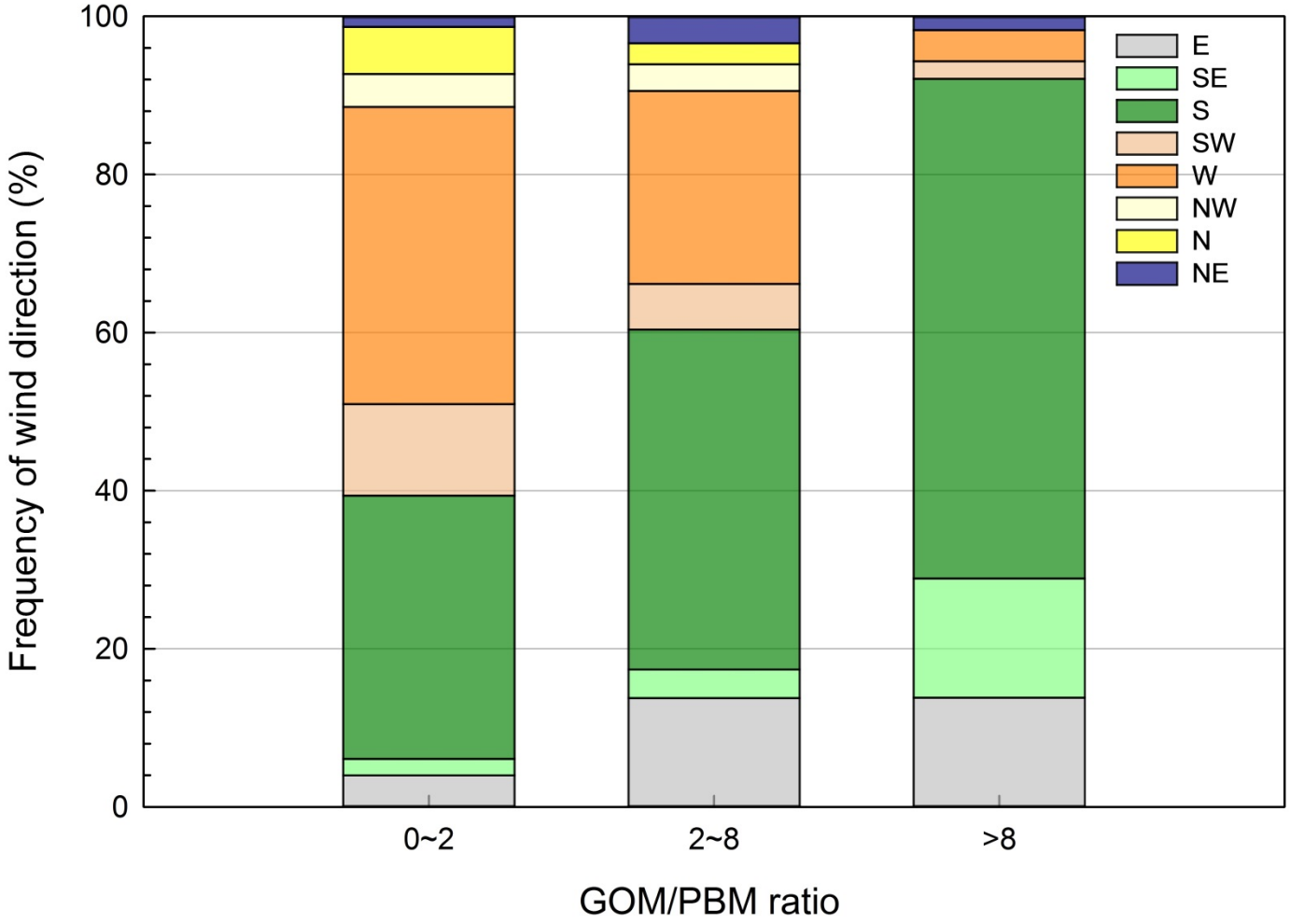

Figure 6. Frequency of wind direction with different GOM/PBM ratios. Southerly and easterly winds prevailed for the samples with high GOM/PBM ratio whereas the percentage of westerly winds increased as the GOM/PBM ratio decreased.

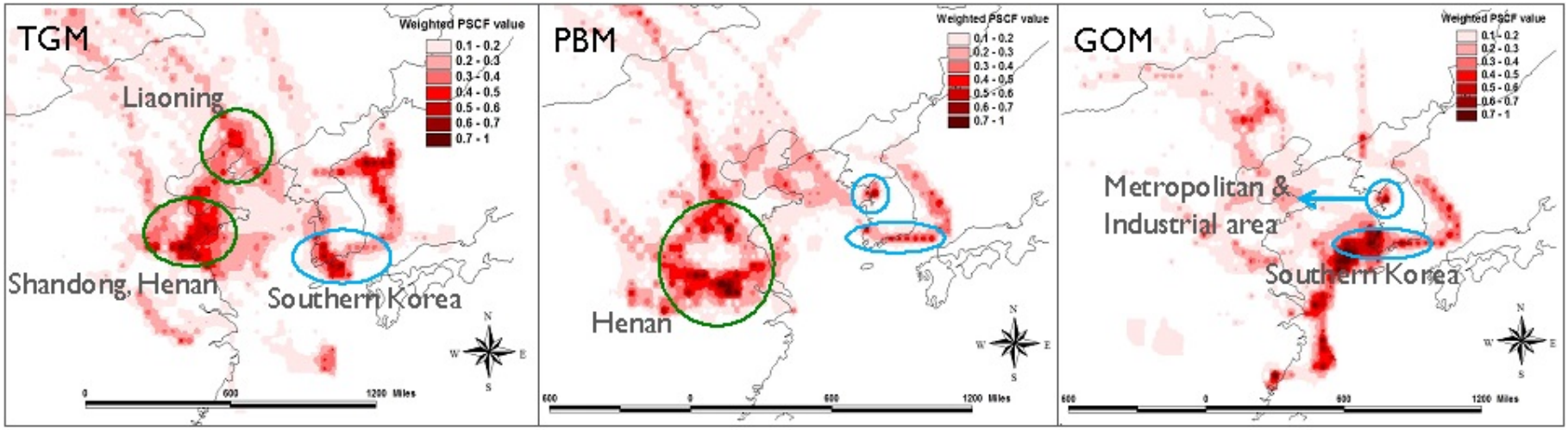

Figure 7. PSCF results for TGM (left), PBM (middle), and GOM (right) using the top 25% of concentrations as criteria.

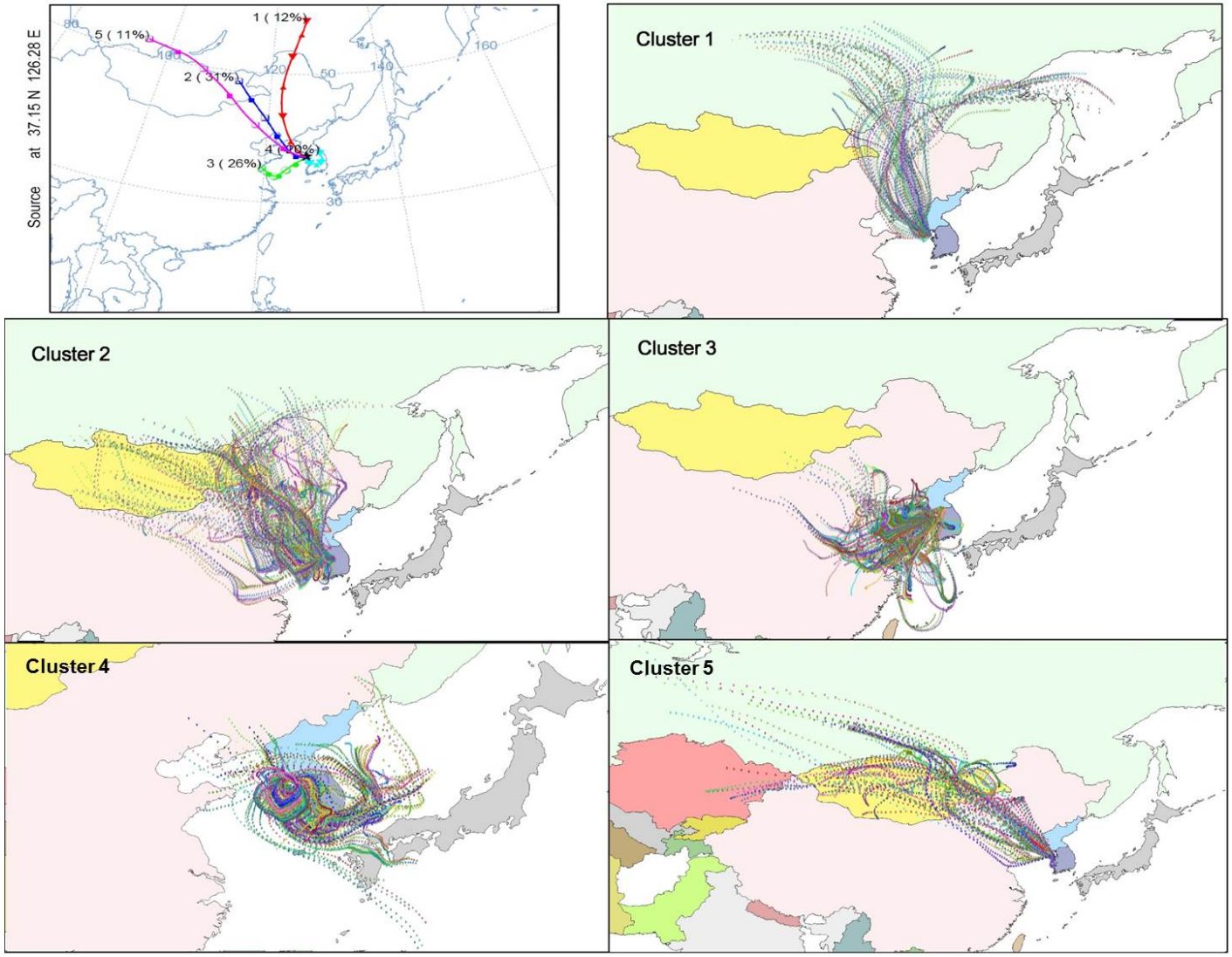

Figure 8. Back-trajectories for clusters 1 through 5. The left top panel indicates the mean back-trajectory and contribution for each cluster.